

Size and shape-dependent electron–hole relaxation dynamics in CdS nanocrystals

Rupa Sarkar, Ajay Kumar Shaw, S. Shankara Narayanan, Carsten Rothe¹,
Susanne Hintschich¹, Andy Monkman¹, Samir Kumar Pal^{*}

*Unit for Nano Science and Technology, Department of Chemical, Biological & Macromolecular Sciences,
S.N. Bose National Centre for Basic Sciences, Block JD, Sector III, Salt Lake, Kolkata 700 098, India*

Received 22 April 2006; received in revised form 25 May 2006; accepted 16 June 2006
Available online 1 August 2006

Abstract

The dynamics of photoluminescence (PL) in CdS nanocrystals (NCs) with various sizes and shapes dispersed in water-in-oil micro-emulsions (reverse micelles) are studied with picosecond-resolved time correlated single photon counting (TCSPC), streak camera and nanosecond resolved gated PL spectroscopic techniques. The time resolved PL-spectra exhibit several discrete features, which are not pronounced in steady state PL spectra. In quantum dots (QD), slower carrier recombination dynamics are observed in smaller sized NCs. The relaxation of the excited state carriers in a quantum rod (QR) is found to be slower at early time and faster in the longer time scales compared to those in QD with similar volume. The signature of thermoluminescence (TL) of CdS-QR in low temperature (77 K) is clearly evident from our studies. We also study the effect of the shape of the NCs on their PL anisotropy. The steady state and time resolved PL anisotropy of a QR show significantly different behavior compared to those of a QD with similar volume. The results of the NCs are important in the context of designing better, more effective physical and biological PL probes.

© 2006 Elsevier B.V. All rights reserved.

Keywords: Picosecond to microsecond dynamics; Charge carriers of nanocrystal; Quantum dot; Quantum rod; Thermoluminescence; Photoluminescence; Emission anisotropy

1. Introduction

Quantum dots (QD) are luminescent nanometer sized crystals made from semiconductor material [1]. As in an optical waveguide, which must be at least the same size as the wavelength of light in order to confine the light, the extent of the confining potential of a QD should be in the order of the carriers it confines. The effective wavelength of the carriers is the de Broglie wavelength, which in a typical semiconductor lattice at room temperature is about 10 nm [2] and consequently, this is the typical scale of a semiconductor QD. The small size of the confining potential leads to the presence of discrete states, which is

one of the central characteristics of QDs. They are therefore also named “artificial atoms” [2]. The size dependent optical properties of the QDs make them ideal candidates for tunable absorbers and emitters in various applications ranging from nanoelectronics [3–5] to biological fluorescent labeling [6,7].

Recently, there has been a major growth of activities in the synthesis of new QDs of different sizes and shapes [8] including chemical routes of synthesis, which allow fabrication of QDs in the range from 1 nm to 10 nm. The chemical methods are particularly well developed for II–VI semiconductor QDs. The two main chemical routes for preparation of these QDs are high-temperature precipitation in molten glasses [9,10] and colloidal synthesis using, e.g. reverse micellar technique [11–15]. The characterization of the physical properties of the nanocrystals is also one of the interests of current research. Particularly, efforts are focused on under-

^{*} Corresponding author. Fax: +91 33 2335 3477.

E-mail address: skpal@bose.res.in (S.K. Pal).

¹ Department of Physics, University of Durham, UK.

standing the dynamics of charge carriers of the nanoparticles, as all descriptions of quantum-well, -wire, and -box lasers [16–18] rely on the relaxation of the carriers to the ground state. A lot of attention has been paid to the carrier dynamics in II–VI semiconductor (CdSe, CdS, etc.) QDs using femtosecond resolved nonlinear spectroscopy [8,19–22], as they have potentiality in biophysical labeling [6,7]. From the femtosecond resolved temporal studies on the QDs it is clear that after fast energy redistribution, carrier relaxation in bulk II–VI semiconductors proceeds primarily by radiative decay due to enhancement of nonradiative processes associated, e.g. with surface trapping [23,24] and/or multiple Auger recombination [25,26]. It is also evident from the earliest temporal emission studies that a significant portion of the dynamics leftovers in the sub-nanosecond to several hundred-nanosecond time scales, which remains beyond the experimental window of the femtosecond resolved spectroscopic studies [8,21].

However, in order to use the fluorescent QDs in the slower biological events it is extremely important to explore the picosecond to microsecond dynamics of the QDs. One of the recent studies [27] on biologically compatible CdSe quantum dots addressed the issue and explored the time-scales of the QD in various environments. As evidenced in the recent literatures of CdS-QDs, which are in a class of II–VI semiconductor nanocrystals are also important for photocatalytic activity [15] and biophysical studies [28,29]. Some efforts have been given to understand the carrier relaxation dynamics using nanosecond resolved photoluminescence measurement [28,30–32]. However, a study involving picosecond to microsecond dynamics of the charge carriers of CdS quantum dots is still lacking in the recent literatures.

To date, very few results have been published in the picosecond resolved photoluminescence (PL) anisotropy of semiconductor quantum dots of different shapes, although theoretical calculations to predict anisotropy of a QD with wurtzite crystal structure have been advanced [33]. A recent study [34] on CdSe/ZnS nanoparticles in toluene at 300 K shows a time dependent anisotropy, whose time behavior is consistent with the parameters of Brownian rotational motion of the nanocrystals (NCs) in an isotropic liquid. Nevertheless, no result has been published in picosecond resolved PL anisotropy of CdS quantum dots of different shapes.

In this contribution, we report our studies on the carrier dynamics of CdS quantum dots from picosecond to microsecond time scales using time resolved PL measurement techniques. The nanocrystals with various sizes and shapes were made using colloidal solutions of reverse micelles. In order to obtain picosecond resolution we have used time correlated single photon counting (TCSPC) and ultrafast streak camera measurements. The picosecond resolved TCSPC techniques is also employed to study time resolved anisotropy of the NCs of different shapes. The temporal evolution of the PL of the NCs up to several microsecond time window is measured using sub-nanosecond resolved gated spectroscopic technique. We also studied the effect

of temperature (from room temperature to 77 K) on the PL of the NCs of various sizes and shapes.

2. Materials and methods

2.1. Sample preparation

CdCl₂, Na₂S, bis(2-ethylhexyl)sulfosuccinate sodium salt (AOT), hexametaphosphate (HMP) and L-Lecithin were purchased from Sigma (USA) and isooctane from Romil (UK). All the samples were used as received without further purifications. The synthesis of NCs of various sizes was carried out [12] by mixing two AOT reverse micellar ([AOT] = 100 mM) solutions with the same ratio (w_0) of water ($w_0 = [\text{H}_2\text{O}]/[\text{AOT}]$), one containing a solution in which sulfide ions (Na₂S in 100 mM aqueous solution of HMP) were solubilized and the other in which cadmium ions (Cd(NO₃)₂ in aqueous solution) were present. The respective concentrations are, in general, the same $5 \times 10^{-4} \text{ M L}^{-1}$. The mixing is produced by rapid injection of variable volume of solutions of cadmium ions and sulfide ions of same concentration. The final ratio of $[\text{Cd}^{2+}]/[\text{S}^{2-}]$ in the solution was maintained to be 2:1. The nanocrystals of various sizes were obtained by changing w_0 value of the reverse micellar solutions [12]. Transmission electron microscopy (TEM) studies [35] on the NCs prepared following the above method ($w_0 = 10$) reveal particle with spherical morphology (average size $5.01 \pm 0.59 \text{ nm}$). The preparation procedure for quantum rod (QR) is analogous to that of Refs. [35,36]. The synthesis is similar to that of Ref. [12] except that mixed micelles ($w_0 = 10$) of AOT and lecithin (0.05 M/0.05 M) and CdCl₂ salt as the source of Cd²⁺ ions were used in the latter case. As found in the literature [35,36] the CdS particles are needle like (quantum rod, QR) in appearance with an average width of $4.15 \pm 0.63 \text{ nm}$ and average length $48.68 \pm 5.48 \text{ nm}$. In the following sections we will refer NCs with spherical morphology as quantum dot (QD). QDs in the AOT reverse micelles (RM) of $w_0 = 5, 10$ and 20 will be referred as QD5, QD10 and QD20, respectively. The quantum rod (QR) in the RM of $w_0 = 10$ will be referred as QR10.

2.2. Steady state and time correlated single photon counting measurement (TCSPC)

Steady-state absorption and emission were measured with Perkin Elmer lambda19 spectrophotometer and a Jobin Yvon Fluorolog-2 fluorimeter, respectively. All transients were taken by using picosecond-resolved time correlated single photon counting (TCSPC) technique. The system uses a picosecond diode laser and Becker & Hickel electronics; it has an instrument response function (IRF) $\sim 90 \text{ ps}$. The picosecond excitation pulse from picosecond diode laser was used at 388 nm. A liquid scatterer was used to measure the FWHM of the instrument response functions (IRF). The fluorescence from the sample was detected by a micro-channel plate photomultiplier

tube (MCP-PMT, Hammamatsu) after dispersion through a grating monochromator. For all transients the polarizer in the emission side was adjusted to be at 54.7° (magic angle) with respect to the polarization axis of the excitation beam.

The observed fluorescence transients were fitted by using a nonlinear least squares fitting procedure (software SCIENTIST) to a function comprising of the convolution of the instrument response function with a sum of exponentials. The purpose of this fitting is to obtain the decays in an analytic form suitable for further data analysis. For anisotropy measurements, emission polarization was adjusted to be parallel or perpendicular to that of the excitation and anisotropy defined as $r(t) = [I_{\text{para}} - G \cdot I_{\text{perp}}] / [I_{\text{para}} + 2 \cdot G \cdot I_{\text{perp}}]$. The magnitude of G , the grating factor of the emission monochromator of the TCSPC system was found by using a coumarin dye in methanol and following longtime tail matching technique [37] to be 1.1.

2.3. Streak camera

Picosecond emission spectroscopy was achieved using a streak camera setup. Samples are excited at 365 nm (3.4 eV) by a frequency doubled Ti:Sapphire laser (Mira 900, Coherent) with an output pulse width of less than 2 ps and a repetition rate of 76.3 MHz. Perpendicular to the excitation path, the sample emission was passed through a monochromator (Acton Spectra Pro 2300i), and finally, the emission spectrum is detected by the photocathode of a Hamamatsu streak camera (C5680). In these settings, the scattered excitation beam was observed with a half pulse width of 20 ps, which corresponds to the overall time resolution of the setup. This exceeds the laser pulse width because, for the presented experiments, the sweep speed of the streak apparatus was set as slow as possible in order to monitor sample emission as far as 2 ns. A spectral resolution of 4 nm has been determined using an argon calibration lamp. Finally, all images are corrected for curvature, shading and spectral response via computer. Spectra at fixed points in time were then read out as profiles of a specified image section.

2.4. Gated spectroscopy

Time-resolved emission detection covering the nano, micro, and millisecond time domain was accomplished using a gated spectroscopy setup. Here, the frequency-tripled output of a 160 ps pulsed Nd:yttrium aluminum garnet laser was used for optical excitation at 3.5 eV (355 nm). Images of the spectrographically dispersed sample emission were detected by an intensified CCD camera (4 Picos, 100 ps smallest time step). These spectra are characterized by two tunable time periods: the time after pulsed excitation until the start of the light detection (delay time) and the duration of the light detection (integration time). In order to obtain decay kinetics, each spectrum was integrated over the desired energy region and plotted versus the

appropriated time. The overall one nanosecond time resolution of this setup is accompanied by a very large dynamic range, thus, luminescence decays can be traced for significantly longer time periods than with other experiments; details are given in Ref. [38]. A temperature controlled duplex helium cryostat additionally allowed to vary the temperature between room temperature and 11 K. In the present study we have used liquid nitrogen to attain sample temperature at 77 K.

3. Results and discussion

CdS nanocrystals in the reverse micellar (RM) suspensions are characterized by absorption spectra (Fig. 1a). As described in the early studies [39–41], the quantum effect of size of the nanocrystals (NCs) is clearly evident. It results in a perturbation of the electron structure of the semiconductor due to change in the particle size. This gives a widening of the forbidden band (band edges) and therefore a shift of the shoulder in the spectrum as the size decreases. The continuous increase in the absorption below the wavelength corresponding to the shoulder is consistent with absorption in the conduction bands with relatively higher energies. An attempt has been made to correlate average size of the nanocrystals in the solutions estimated from photoabsorption threshold to the size of the aqueous water pool of the host RM [12,41]. The radius of the aqueous pool in angstrom was obtained from the empirical formula, $r_0 = 1.5 \times w_0$, where w_0 was defined as the ratio of molar concentrations of water and AOT in the RM solutions [12]. From the above studies it has been concluded that the sizes of the aqueous water pools of small host RM ($w_0 \leq 10$) matched with the sizes of the nanocrystals estimated from their corresponding photoabsorption threshold [12].

In Fig. 1b, the excitation spectra of the CdS-QD formed in a RM of $w_0 = 10$ is shown. Definite peaks in the spectra and small shift in the peak position with various detection wavelengths (420 nm, 500 nm and 580 nm) indicate a significant optical transition from the edge of the conduction band. Reasonably small excitation wavelength dependency of the emission spectra as shown in Fig. 1c confirms narrow dispersion in the CdS size in the RM [12,28]. Fig. 2a shows absorption spectrum of a QR10 (solid line). The shoulder (~ 320 nm) in the absorption is quite blue shifted compared to that of the QD10 (365 nm) of similar volume indicating optical properties are highly dependent on the shape of the nanocrystals. X-ray diffraction studies [35] on the similar QD and QR with high aspect ratio reveal a significant change in particle morphology, along with the shape. The study [35] shows that the crystal structure of the QD is predominantly cubic whereas the structure of the QR is hexagonal in nature. The change of the crystal structure of QR compared to that of QD could be one of the reasons for altered optical transition affecting the absorption spectrum of QR. In contrast to the QD, the excitation spectra (Fig. 2b) of QR show significant dependency on the

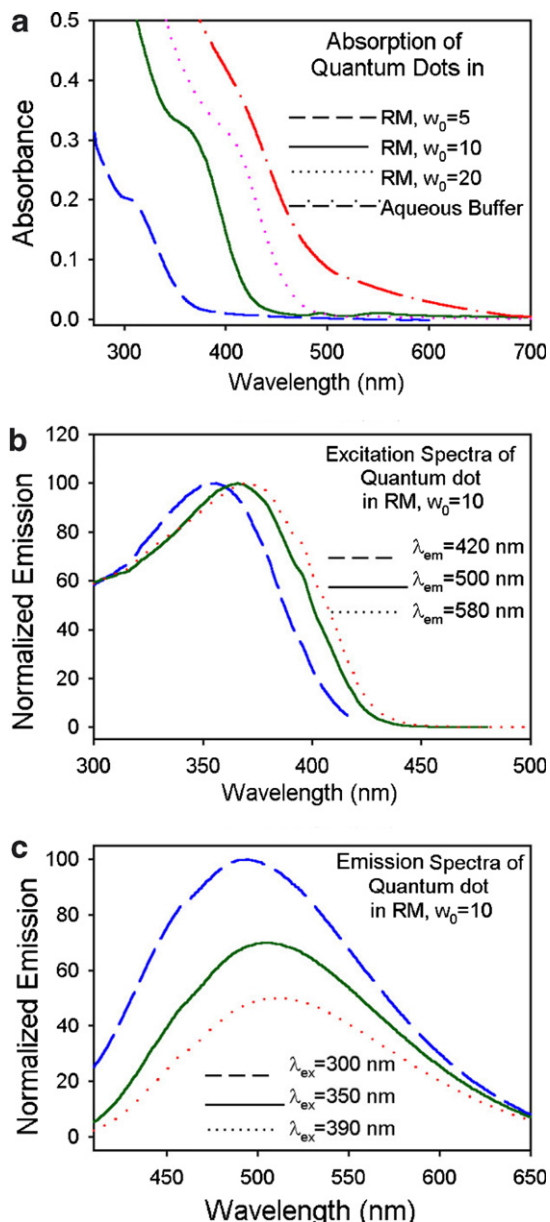


Fig. 1. (a) Absorption spectra of quantum dots with various sizes are shown. Note the shift of the shoulder of the absorption towards blue region as the size of the nanoparticles decreases. (b) Excitation spectra of the quantum dot in the reverse micelle of $w_0 = 10$ in various emission wavelengths. (c) Emission spectra of the quantum dot in the reverse micelle of $w_0 = 10$ in various excitation wavelengths. In the preparation of the CdS-NCs, Na_2S in 100 mM aqueous solution of HMP buffer and $\text{Cd}(\text{NO}_3)_2$ in pure water were solubilized (see text).

wavelength of detection (420 nm, 470 nm and 580 nm). The feature of each spectrum along with the wavelength dependency of the excitation spectra indicate the optical transitions from various excited states. We made sure that the sharp features in the excitation spectra below 400 nm are not due to spectral characteristics of the excitation Xe lamp. The excitation wavelength-dependent eventual emission spectrum of the QR (Fig. 2c) also supports the above conjecture. It is well-known that the mixing of valence bands in spherical II–VI semiconductors, particularly in CdSe nano-

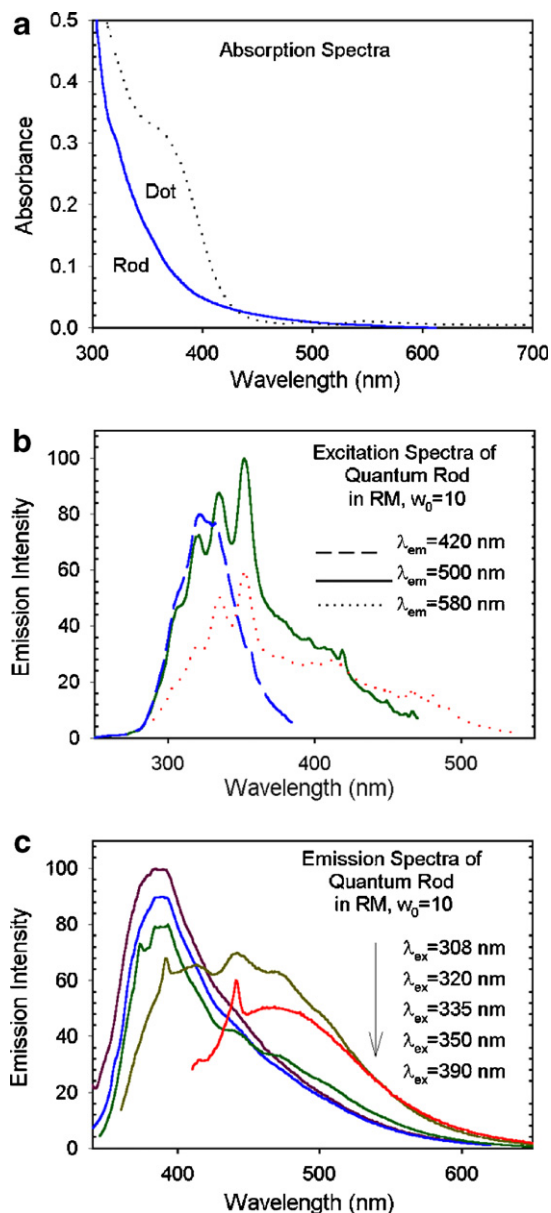


Fig. 2. (a) Absorption spectrum of quantum rod (solid line) is shown. The absorption spectrum of quantum dot in the RM ($w_0 = 10$) is also shown for comparison. (b) Excitation spectra of the quantum rod in the reverse micelle of $w_0 = 10$ in various emission wavelengths. (c) Emission spectra of the quantum rod in the reverse micelle of $w_0 = 10$ in various excitation wavelengths.

crystals is a very important factor controlling their optical properties [42,43]. For example, in CdS-QRs, the symmetry breaking caused by the elongation modifies the band-mixing in such a way that each eigenstate has a definite component of total angular momentum along the long axis [44]. The difference in steady state optical properties, particularly blue shift of QR absorption/emission spectrum compared to that of the QD is thought to be an indication that the quantum confinement length is primarily defined by the particle width. It is also possible that surface state saturation is modified by particle–surfactant interactions,

which may differ between the single surfactant case (QD) and the mixed surfactant case (QR).

The time resolved emission spectra of CdS nanocrystals with various sizes and shapes are shown in Fig. 3. The QDs in the RM of $w_0 = 10$, average diameter ~ 5 nm [35] shows much faster decay in the blue end of the emission spectrum (high energy) as evident from the streak camera measurements (Fig. 3a). In contrast, the larger sized QD (in $w_0 = 20$ RM) shows almost uniform decay in all emission wavelengths as shown in Fig. 3b. The time resolved emission of the QR as shown in Fig. 3c shows many peaks sim-

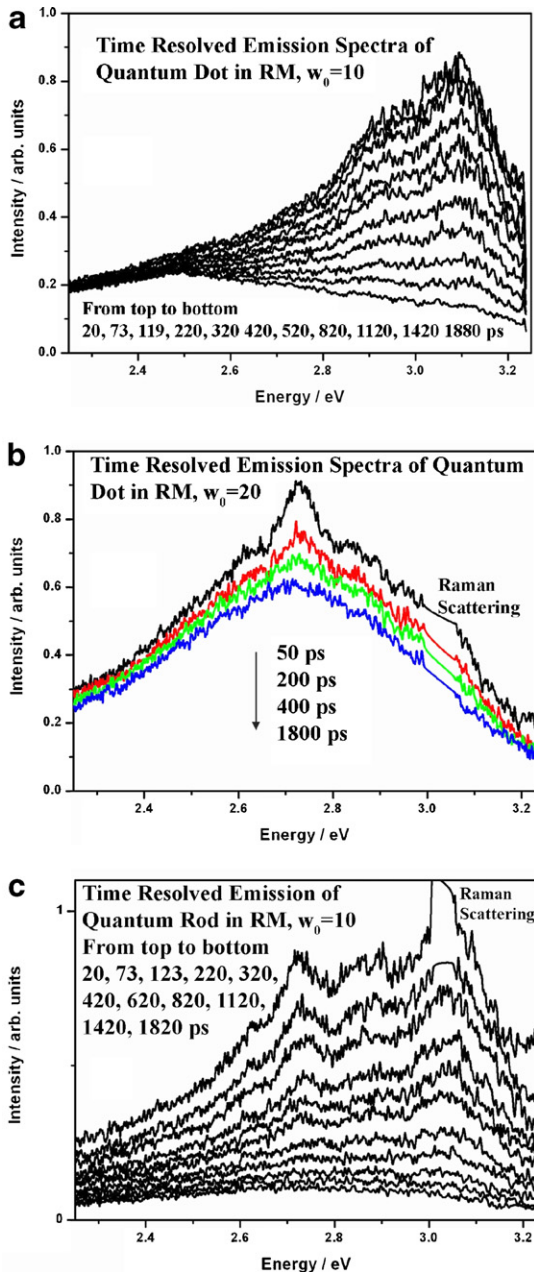


Fig. 3. The time resolved emission spectra obtained from a picosecond resolved Streak camera for QD10 (a), QD20 (b) and QR10 (c) are shown (see text).

ilar to the steady state spectrum of the QR (Fig. 2c). The blue end of the emission spectrum decays relatively faster than that in the red side of the spectrum.

In order to get the picosecond resolved emission transients of the QDs with various sizes and QR nanocrystals we also performed TCSPC measurements on those systems. As shown in Fig. 4a blue side of the emission spectrum of QD10 shows faster decay (125 ps (62%), 750 ps (27%) at 420 nm) compared to those in peak (302 ps (54%) and 1.26 ns (21%) at 500 nm) and red edges (522 ps (48%) and 1.61 ns (21%) at 620 nm; 572 ps (47%) and 1.77 ns (21%) at 640 nm) of the steady state spectrum. The emission decay at the peak wavelength (235 ps (46%) and 1.12 ns (35%) at 560 nm) of QD20 is similar to that of the QD10. However, long time constants, which do not decay significantly within the 15 ns time window, are clearly evident in the 300 ns experimental window (Fig. 4b). The fitted longest lifetime of the QD10 at 500 nm and QD20 at 560 nm are found to be 112 ns and 91 ns, respectively. The longest time constant for the QD10 at 640 nm was 123 ns.

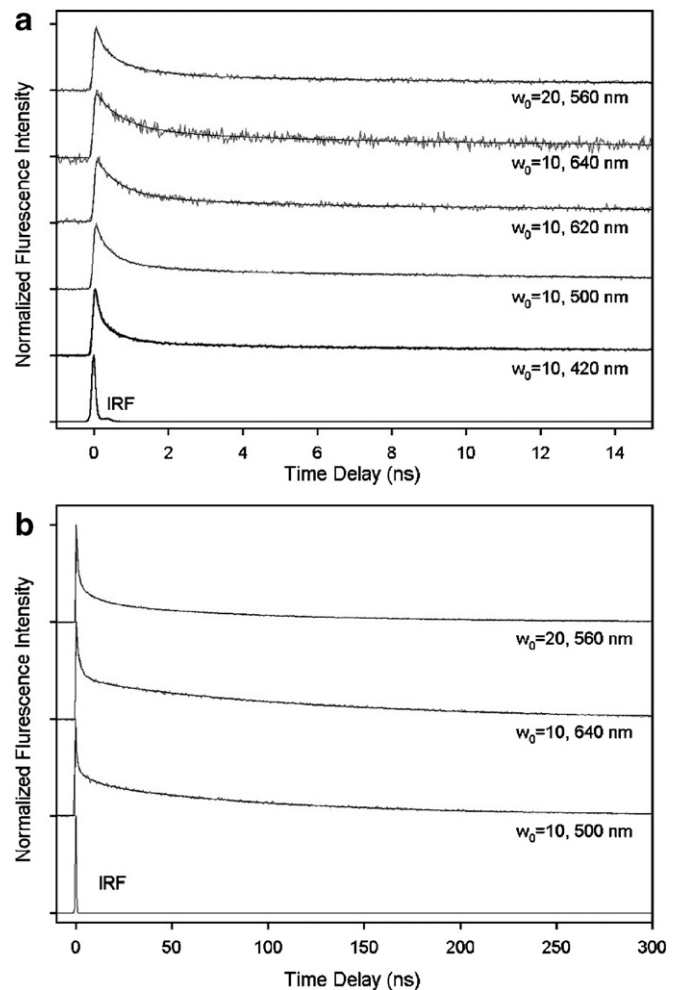


Fig. 4. Time resolved photoluminescence transients of quantum dots with various sizes detected at different wavelengths in shorter (a) and longer (b) time windows.

To date, no detailed physical or mathematical model has been advanced to describe emission dynamics of NCs. From previous theoretical and experimental ultrafast photoluminescence (PL) studies [8,21] the dynamics of the carrier recombination as evidenced from our time resolved experiments following statements can be made. Excitation of II–VI semiconductor nanocrystals promotes an electron from valence to conduction band, which can then undergo radiative relaxation. The intra-conduction band relaxation of the carrier electron is thought to be dominated by the interactions with longitudinal optical (LO) phonon modes, leading to fast (sub-picosecond) nonradiative relaxation in the dynamics. In the nanocrystals even with relatively larger dimension i.e. in the region of weak carrier confinement, when level spacing is only few millielectron volts, the carrier relaxation mediated by interactions with LO, is hindered dramatically because of the restriction imposed by energy and momentum conservation leading to a phenomenon called “phonon bottleneck” [21]. In the NCs with relatively smaller diameter (stronger quantum confinement) further reduction in the energy loss rate is expected, for which the level spacing can be much greater than LO phonon energies, and hence carrier phonon scattering can only occur via weak multi-phonon processes.

In our experiments relatively faster early dynamics in QD20 (235 ps and 1.12 ns) compared to that in QD10 (302 ps and 1.26 ns) could have some relevance to the phonon bottleneck effect. However, the controversial existence of the phonon bottleneck effect as evidenced in a number of recent experiments on II–VI nanocrystals is clearly discussed in Ref. [21]. Another possibility of the faster dynamics in the larger NCs could be due to nonradiative relaxation to underlying trap states [8]. In the NCs uncoordinated surface atoms give rise to trap states that lie within the band gap and reduce quantum yield by providing alternative pathways of excited state relaxation. For example, in CdSe-NCs decay component of sub-100 ps is recovered in the transient absorption signal, which is concluded to be due to the trapping at the surface defect [8]. The faster photoluminescence decay in the larger sized NCs may also be due to volume recombination of the carriers [45] in the bulk semiconductor, as the surface to volume ratio decreases with the size of the NCs.

In Fig. 5, picosecond resolved PL transients of CdS quantum rod (QR10) in short (Fig. 5a) and long (Fig. 5b) time windows are shown. The transients of QD10 are also shown for comparison. The transients of QR10 show two major time constants of 420 ps (70%) and 2.89 ns (28%), which are slower than those of the QD10. In contrast to the case of QD10, QR10 shows negligibly small contribution of longer time constant (56 ns, 2%). Earlier, femtosecond resolved transient absorption studies on the CdSe-NCs reveal that within 200 fs the carriers seem to distribute themselves among fewer energy states in the dots compared to the rods [8]. The existence of more emissive states in QR10 compared to QD10 is clearly seen from our steady state excitation and emission

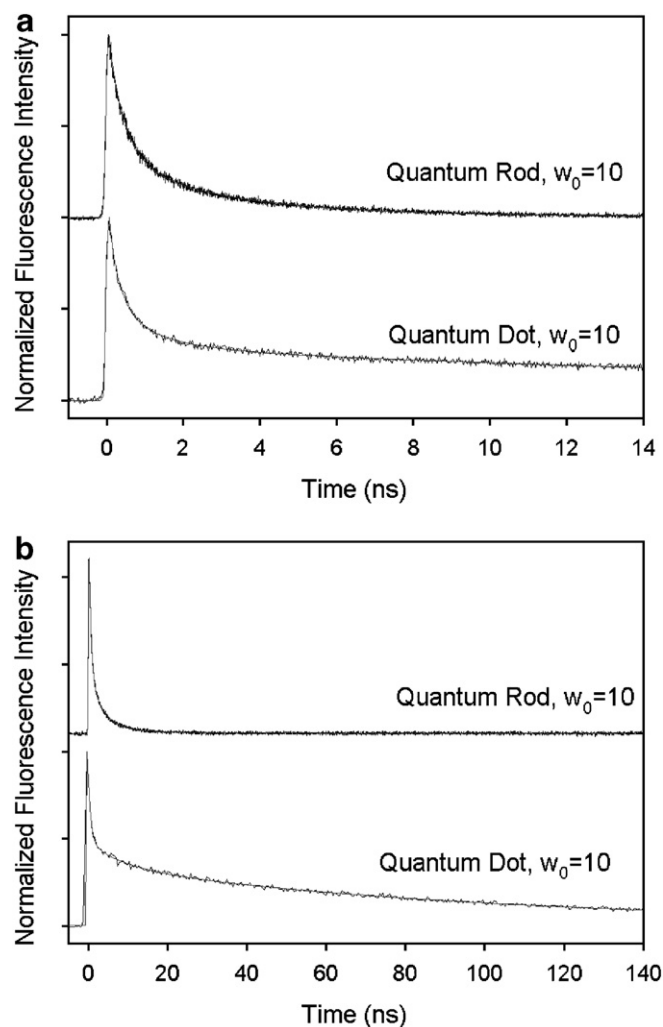


Fig. 5. Time resolved photoluminescence transients of quantum rod in shorter (a) and longer (b) time windows are shown. The transient of the quantum dot is also shown for comparison.

studies (Figs. 1 and 2). From the emission spectrum of QR10, a blue shift compared to that of the QD10 is also evident. The cause for the blue shift is thought to be an indication that the quantum confinement length is primarily defined by the particle width and its difference between the widths of the sphere and the rods. Although, other possibility of the presence of mixed surfactant in QR10 for the blue shift cannot be ruled out completely.

In the case of higher confinement of carriers in the QR10, the slower time constants in the early time (420 ps and 2.89 ns), are consistent, given the inefficient electron–phonon coupling in the QR10 compared to that in QD10 [21]. The negligibly small contribution of the slower time constant (56 ns, 2%) in the QR10 compared with that in the QD10 could be explained by the fact that lowering the symmetry in the rods leads to splitting of the degeneracy of the energy levels in the rods. It should be mentioned that the increase in the density of states leads to an increase in the relaxation process involving either electron–phonon or electron–hole coupling [46]. The smaller the electron

energy separation, the more likely phonons/holes can be found to accept the released energy, and thus, the faster overall relaxation.

In order to follow carrier dynamics in the QD of various sizes and QR10, nanosecond resolved gated emission spectroscopy have been performed. As shown in Fig. 6, the temporal behavior of the PL of QD10 (Fig. 6a) is significantly different compared to that of QD5 (Fig. 6b), particularly in the blue region of the spectra. Longer time the emission spectra of QD10 become narrower than that of QD5, indicating emission from fewer emitting energy states in the former case. The narrow bandwidth in the emission spectrum of QD10 compared to that of QD5 also indicate essentially band edge emission following faster intra-band relaxation due to efficient electron–phonon/hole coupling. In the case of larger QDs, e.g. CdS in the RM with

$w_0 = 20$ and in aqueous buffer, the emission spectra show many temporal features as shown in Fig. 7. For both the samples two distinct emission bands in the early time (up to 3 ns) are observed. As time progresses, bands at higher energy reduce their weight to give single peaks in the red side (low energy) of the spectra. The existence of the two peaks in the emission spectra could be due to significantly large polydispersity in the sizes of the NCs. The time evolution of the emission spectra of QR10 is qualitatively similar to that of QD10 giving relatively narrower spectrum in the longtime (Fig. 8).

In order to investigate the nature of energy structure of the emitting states, temperature dependent gated spectroscopy experiments have been performed on the NCs. Fig. 9 shows time resolved emission spectra of QD10 (Fig. 9a) and QR10 (Fig. 9b) at 77 K. The temporal behavior of

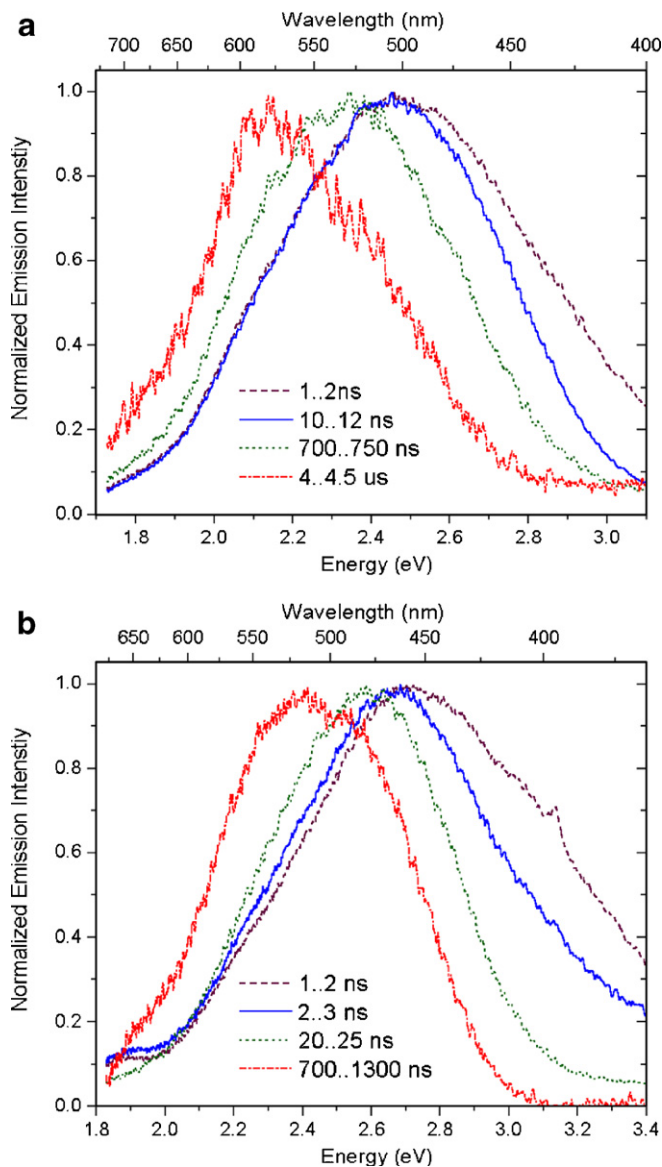


Fig. 6. Time resolved spectra obtained from nanosecond resolved gated photoluminescence spectrometer for QD10 (a) and QD5 (b) at 300 K are shown (see text).

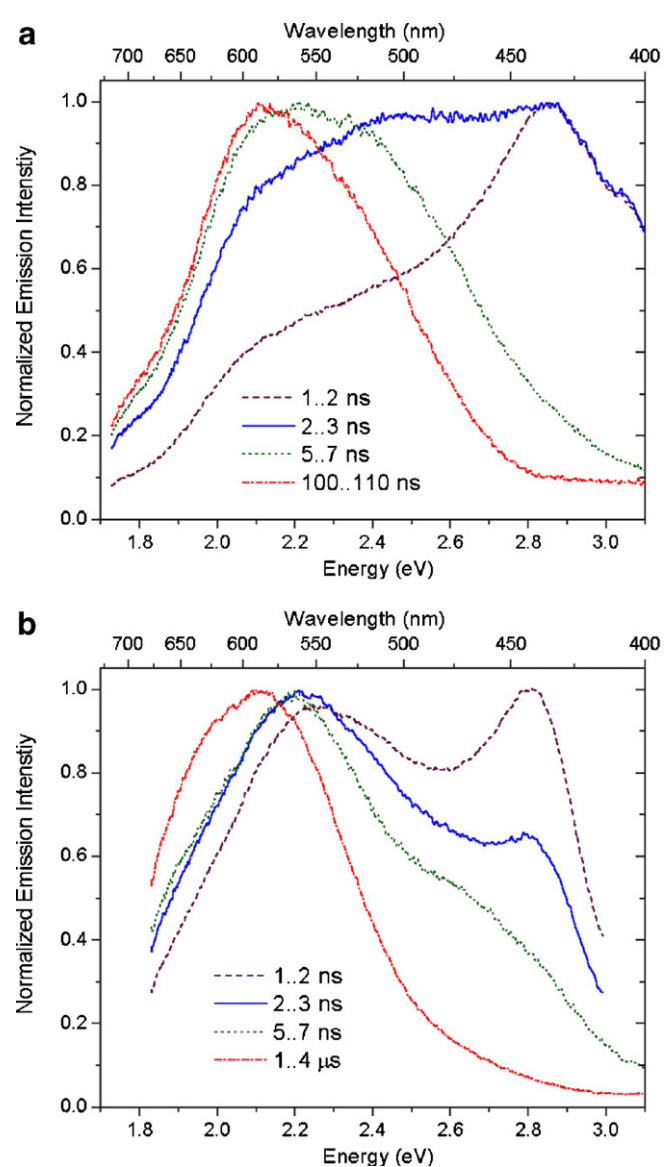


Fig. 7. Time resolved spectra obtained from nanosecond resolved gated photoluminescence spectrometer for QD20 (a) and quantum dot in aqueous environment (b) at 300 K are shown (see text).

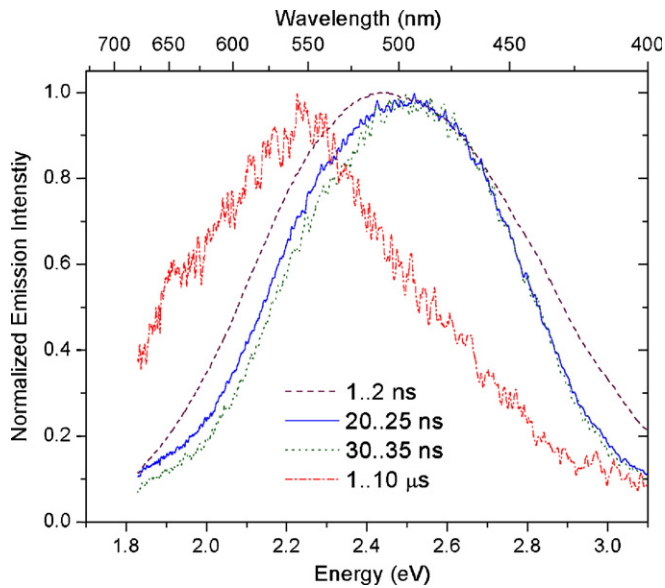


Fig. 8. Time resolved spectra obtained from nanosecond resolved gated photoluminescence spectrometer for QR10 at 300 K are shown (see text).

the QD10 at low temperature is similar to that at room temperature give comparatively narrower spectrum at 40–140 μs , which indicate the emission to be from essentially one state. However, the nature of the temporal spectra of QR10 at early time (1–2 ns) is significantly different from that at later time (1–10 μs). The main peak of the spectrum at 1–10 μs is significantly red-shifted and a shoulder at the position of the peak at early time (1–2 ns) is clearly evident. At 77 K the spectral signature of the QR10 at later time (after ~ 10 ns) is different from that in the room temperature, but consistent with the emission from two emitting states. The phenomenon could be a clear demonstration of the thermoluminescence (TL) in the QR10 [8]. It is known that following photoexcitation, electron hole pairs (EHP) are created in the semiconductor NCs. If the photo-excited EHP recombine immediately and emit a photon that is known as fluorescence, and if the EHP does not recombine rapidly, but are trapped in some metastable states separately, they need energy to be released from the traps and recombine to confer delayed luminescence. If they spontaneously recombine after sometime, it is called photoluminescence (PL). The detrapping process caused heating is known as thermostimulation. The shoulder peak in the emission spectrum of QR10 at low temperature clearly indicates one of the trapped states, which can easily be thermostimulated at room temperature. On the other hand, no evidence of thermostimulation is found in QD10.

Fig. 10 shows steady state PL anisotropy spectrum (anisotropy versus wavelength of detection) of QD10 (Fig. 10a) and QR10 (Fig. 10b) with various excitation wavelengths. The steady state anisotropy of QD10 shows a peak ~ 375 nm at the excitation wavelength of 300 nm. The peak of the anisotropy spectrum is found to be significantly blue shifted compared to the photoluminescence

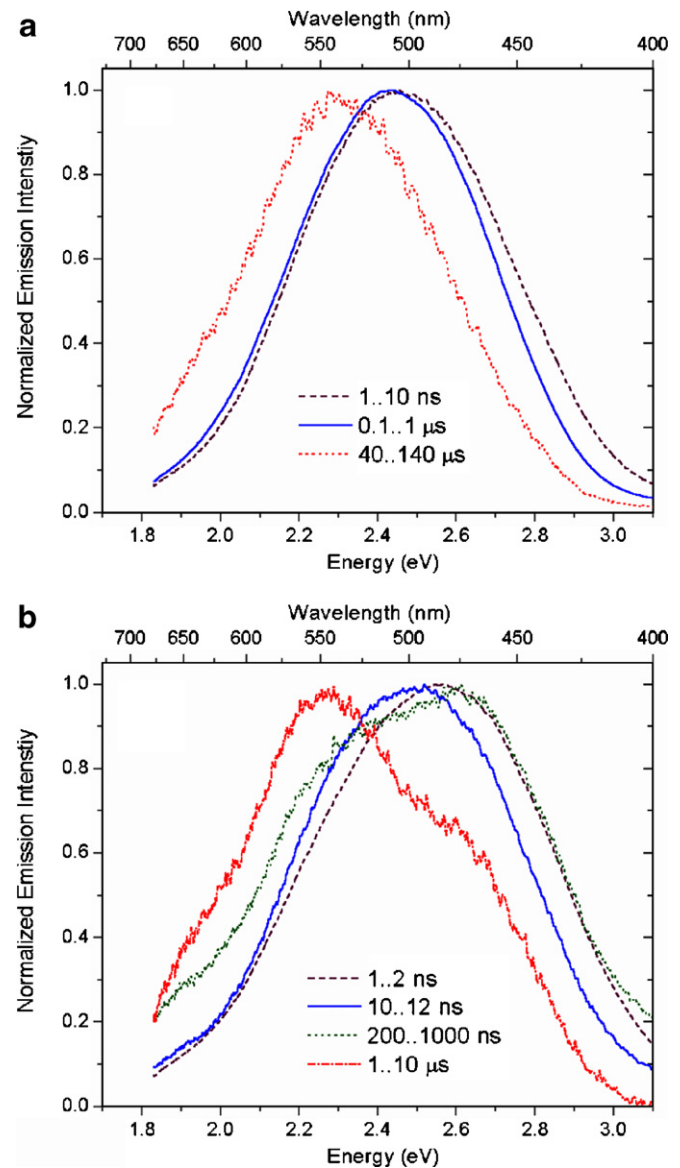


Fig. 9. Time resolved spectra obtained from nanosecond resolved gated photoluminescence spectrometer for QD10 (a) and QR10 (b) at 77 K are shown (see text).

peak (~ 500 nm). The pattern of the steady state anisotropy remains almost similar in all excitation wavelengths (300 nm, 350 nm and 390 nm) giving a small value (~ 0.01) at 500 nm detection as indicated by arrow in Fig. 10a. For QR10 the steady state anisotropy shows a global peak around 375 nm similar to QD10. However, for QR10, when the excitation wavelength is made redder the relative amplitude of the anisotropy is found to increase in all wavelengths of detection. The peak positions in the anisotropy spectra for various excitation wavelengths (300 nm, 308 nm, 320 nm, 350 nm and 390 nm) remain almost similar. At the photoluminescence peak (470 nm, excitation at 390 nm) the value of the anisotropy is ~ 0.2 , which is much higher than that of the QD10 (~ 0.01 , at 500 nm, excitation 390 nm).

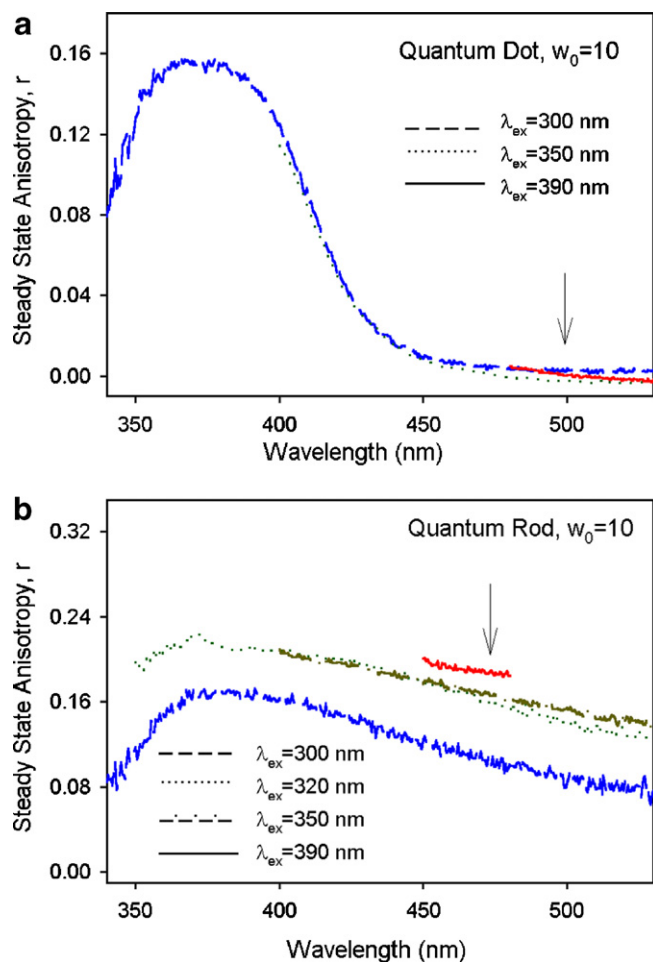


Fig. 10. Steady state PL anisotropy of quantum dot (a) and quantum rod (b) in reverse micelle ($w_0 = 10$) with various excitation wavelengths are shown.

To date, very few experimental works have been published in the steady state and time resolved photoluminescence anisotropy of NCs in a colloidal dispersion (RM). Particularly, no results have been published in the temporal behavior of the anisotropy of CdS-NCs dispersed in RM and the effect of the shape of the NCs on the dynamics of the anisotropy. In recent studies [34,47,48], two possible radiative transitions were found to exist in prolate and unidirectional wurzite II–VI semiconductor crystal structure of CdSe-NCs [47]. The energetically lowest lying transition is an electric transition dipole moment oriented along the wurzite c -axis. However, this transition is optically forbidden. The higher lying optically allowed transition is predicted to be doubly degenerate and should give rise to an isotropic 2D transition dipole lying within the crystallographic a – b plane. Thus if the observed NC photoluminescence is due to this transition, emission of an individual NC should be circularly polarized, which is supported by recent experiments on single NCs [49–52]. In a recent communication [34], photoluminescence anisotropy of CdSe/ZnS colloids in toluene solution at room temperature shows a time dependent anisotropy. The temporal behavior of the

anisotropy is consistent with the parameters of Brownian rotational motion of the NCs in an isotropic liquid and also comparable with related energy states at low temperature. In another study [32] no detectable steady state and time resolved anisotropy was found for polyphosphate stabilized CdS nanoparticle/starburst dendrimer composites showed polarized room temperature photoluminescence with the anisotropy characterized by an initial value of about 0.2 and a correlation time of about 2.4 μ s.

Our observations of the steady state anisotropy of QD10 in the RM are not consistent with that of NCs in toluene at 300 K [34]. The blue shift of the anisotropy peak compared to that of the photoluminescence peak cannot be due to distribution of the particle size in the reverse micellar solution of QD10 as the transmission electron microscopy (TEM) studies [35] on the same system reveals the distribution to be less than 10%. The change in the amplitude of steady state anisotropy of QR10 in all wavelengths of detection with various excitation wavelengths could be due to multiple emitting states present in QR10. The existence of a number of emitting states is also confirmed from our steady state excitation and emission experiments (Fig. 2). Details of the anisotropy spectra of QD10 and

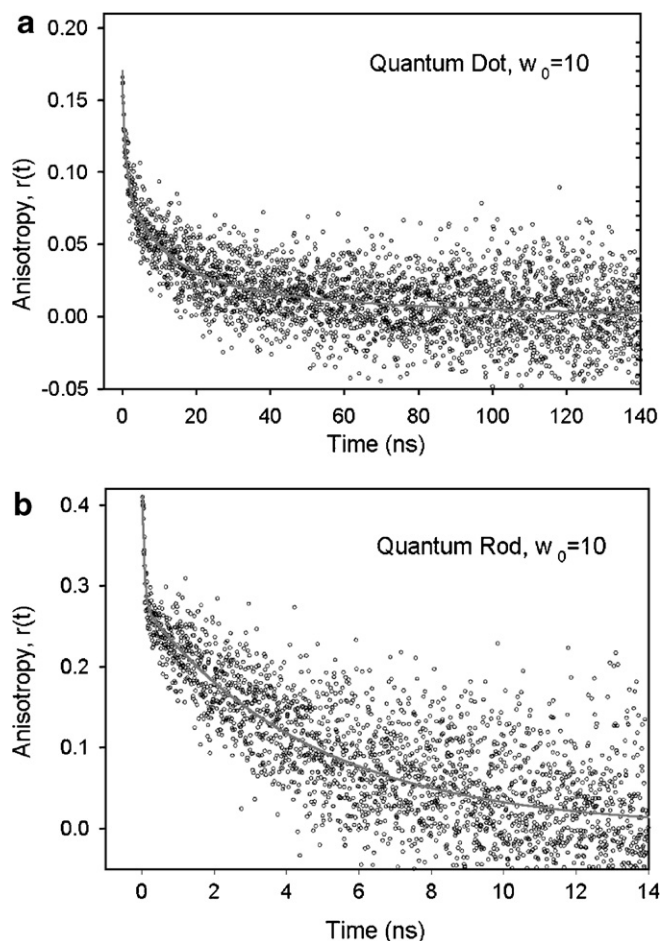


Fig. 11. Picosecond resolved PL anisotropy of quantum dot (a) and quantum rod (b) in reverse micelle ($w_0 = 10$) with 390 nm excitation are shown.

QR10 can only be explained by detail studies on the electronic states of NCs. Work in the direction is in progress in our group.

The temporal behavior of the anisotropy of QD10 (at 500 nm) and QR10 (at 470 nm) are shown in Fig. 11a and b, respectively. The PL anisotropy decay of QD10 shows three distinct time constants (1.05 ns (42%), 10.7 ns (39%) and 57.1 ns (19%)). For QR10 the temporal behavior of the anisotropy shows biexponential nature (~ 50 ps (40%), 4.66 ns (60%)). The anisotropy values of QD10 and QR10 at $t = 0$ (r_0) are found to be 0.17 and 0.7, respectively. Although, as mentioned earlier, details of the temporal behavior of anisotropy of QD10 and QR10 can be understood from theoretical calculation on the energy structures of the NCs, a clear effect of the structural anisotropy of the NCs is evident in the r_0 values. Higher r_0 value of QR10 (0.4) compared to that of QD10 (0.17) distinctly reflects a significant deviation from perfect symmetry in the QR10.

4. Conclusion

Studies of picosecond to microsecond dynamics of CdS nanocrystals (NCs) of various sizes and shapes elucidate photophysical properties of single batch of quantum dots in reverse micelles. After photoexcitation higher energy electron relaxes to the edge of the conduction band through various nonradiative processes e.g. Auger process, optical phonon coupling etc. The rate of the nonradiative intraband relaxation is found to be slower in the smaller sized quantum dots and quantum rods due to higher quantum confinement effect. The band edge energy state can be coupled dominantly with lower lying trap states generated due to surface defects in the nanocrystals. The time resolved photoluminescence transients of the lower energy states i.e. in the red side of the photoluminescence spectrum of the quantum dots do not show any rise component. The observation is consistent with the fact that the population in the trapped state generated from the band edge is also coupled to another lower lying trap state through faster nonradiative relaxation processes. There could be several trapped states, depending upon their depth they can be classified as shallow trap, deep traps and deeper trap, etc. Hole extended states could lie above the valence band (VB) [53]. From our studies we observed emission from several shallow traps with time constants up to 3 ns following ultrafast de-excitation from the edge of the conduction band [22]. The majority of the excited state population (~ 60 – 70%) were found to decay through these shallow traps. The time scales observed in our experiments around 10 ns, 100 ns and 1 μ s can be consequences of shallow trap, deep trap and deeper trap transition respectively, which are in good agreement with Ref. [54].

Size and shape variation study reveals that the variation of the nanoparticle size has insignificant contribution on the relaxation dynamics of the nanoparticle but the dynamics differs with the change of the shape of the nanoparticle

due to change of their quantum confinement. In contrast to the case of QD10 the temperature dependent gated spectroscopy on the QR10 shows the existence of thermoluminescence in the NCs, most probably from shallow trap emitting states. Our steady state and time resolved anisotropy studies on the QD10 and QR10 distinctly show the contribution of shape of the NCs on the nature of the photoluminescence anisotropy of the nanoparticles. However, details of the anisotropy can be understood from the comprehensive theoretical calculations on the energy structures of the NCs, which is in progress in our group.

Acknowledgements

RS, AKS thank UGC and SSN thanks CSIR for their fellowships, we acknowledge financial support from the Durham University Photonic Materials Institute and CEN-AMS (ONE NorthEast).

References

- [1] D. Bimberg, M. Grundmann, N.N. Ledentsov, *Quantum Dot Hetero Structures*, John Wiley & Sons, 1999.
- [2] H. Kalt (Ed.), *Optics of Semiconductor and their Nanostructures*, Springer-Verlag, Berlin, 2004.
- [3] V.L. Colvin, M.C. Schlamp, A.P. Alivisatos, *Nature* 370 (1994) 354.
- [4] B.O. Dabbousi, M.G. Bawendi, O.E.A. Onitsuka, *Appl. Phys. Lett.* 66 (1995) 1316.
- [5] M.C. Schlamp, X. Peng, A.P. Alivisatos, *J. Appl. Phys.* 82 (1997) 5837.
- [6] M.J. Bruchez, M. Moronne, P.E.A. Gin, *Science* 281 (1998) 2013.
- [7] W.C.W. Chan, S. Nie, *Science* 281 (1998).
- [8] C. Burda, X. Chen, R. Narayanan, M.A. El-Sayed, *Chem. Rev.* 105 (2005) 1025.
- [9] A. Ekimov, *J. Lumin.* 70 (1996) 1.
- [10] N. Borelli, D. Hall, H. Holland, D. Smith, *J. Appl. Phys.* 61 (1987) 5399.
- [11] C. Petit, M.P. Pileni, *J. Phys. Chem.* 92 (1988) 2282.
- [12] C. Petit, P. Lixon, M.P. Pileni, *J. Phys. Chem.* 94 (1990) 1598.
- [13] M.P. Pileni, L. Motte, C. Petit, *Chem. Mater.* 4 (1992) 338.
- [14] L. Motte, C. Petit, L. Boulanger, P. Lixon, M.P. Pileni, *Langmuir* 8 (1992) 1049.
- [15] T. Hirai, Y. Bando, I. Komasa, *J. Phys. Chem. B* 106 (2002) 8967.
- [16] Y. Arakawa, H. Sakaki, *Appl. Phys. Lett.* 40 (1982) 939.
- [17] Y. Arakawa, H. Sakaki, M. Nishioka, H. Okamoto, N. Miura, *Jpn. J. Appl. Phys.* 22 (1983) 804.
- [18] Y. Miyamoto, M. Asada, Y. Suematsu, *IEEE J. Quantum Electron.* QE-25 (1989) 2001.
- [19] J.Z. Zhang, *Acc. Chem. Res.* 30 (1997) 423.
- [20] J.Z. Zhang, *J. Phys. Chem. B* 104 (2000) 7239.
- [21] V.I. Klimov, *J. Phys. Chem. B* 104 (2000) 6112.
- [22] A.J. Nozik, *Annu. Rev. Phys. Chem.* 52 (2001) 193.
- [23] V.I. Klimov, D.W. McBranch, *Phys. Rev. Lett.* 80 (1998) 4028.
- [24] M.C. Nuss, W. Zinth, W. Kaiser, *Phys. Rev. Lett.* 49 (1998) 1717.
- [25] M. Ghanassi, M. Schanne-Klein, F. Hache, A. Ekimov, D. Ricard, *Appl. Phys. Lett.* 62 (1993) 78.
- [26] V.I. Klimov, A.A. Mikhailovsky, D.W. McBranch, C.A. Leatherdale, M.G. Bawendi, *Science* 287 (2000) 1011.
- [27] J.A. Kloepfer, S.E. Brandforth, J.L. Nadeau, *J. Phys. Chem. B* 109 (2005) 9996.
- [28] J.R. Lakowicz, I. Gryczynski, Z. Gryczynski, K. Nowaczyk, C.J. Murphy, *Anal. Biochem.* 280 (2000) 128.
- [29] S.K. Kulkarni, A.S. Ethiraj, S. Kharrazi, D.N. Deobagkar, D.D. Deobagkar, *Biosens. Bioelectron.* (2004).

- [30] K. Tomihira, D. Kim, M. Nakayama, *J. Lumin.* 112 (2005) 131.
- [31] L. Cao, S. Huang, S. Lu, J. Lin, *J. Colloid Interface Sci.* 284 (2005) 516.
- [32] J.R. Lakowicz, I. Gryczynski, Z. Gryczynski, C.J. Murphy, *J. Phys. Chem. B* 103 (1999) 7613.
- [33] A.L. Efros, *Phys. Rev. B* 46 (1992) 7448.
- [34] E.P. Petrov, F. Cichos, E. Zenkevich, D. Starukhin, C.V. Borczykowski, *Chem. Phys. Lett.* 402 (2005) 233.
- [35] B.A. Simmons, S. Li, V.T. John, G.L. McPherson, A. Bose, W. Zhou, J. He, *NanoLetters* 2 (2002) 263.
- [36] M.-I.E. Barton, *Synthesis, Functionalization and Surface Treatment of Nanoparticle*, American Scientific Publishers, 2003.
- [37] D.V. O'Connor, D. Phillips, *Time Correlated Single Photon Counting*, Academic Press, London, 1984.
- [38] C. Rothe, A.P. Monkman, *Phys. Rev. B* 68 (2003) 075208.
- [39] L.E. Brus, *J. Phys. Chem.* 79 (1983) 5566.
- [40] L.E. Brus, *J. Phys. Chem.* 90 (1986) 4403.
- [41] A. Henglein, *J. Chim. Phys.* 84 (1987) 1044.
- [42] A.L. Efros, M. Rosen, *Annu. Rev. Mater. Sci.* 30 (2000) 475.
- [43] L.-S. Li, J. Hu, W. Yang, A.P. Alivisatos, *NanoLetters* 1 (2001) 349.
- [44] J. Hu, L.-S. Li, W. Yang, L. Manna, L.-W. Wang, A.P. Alivisatos, *Science* 292 (2001) 2060.
- [45] K.V.S. Rao, B. Srinivas, M. Subrahmanyam: *Photocatalytic reactions over semiconductor based zeolites for organic synthesis: A review*, Research Signpost, Trivandrum, Kerala, India, 2004.
- [46] V. Klimov, P. Haring Bolivar, H. Kurz, *Phys. Rev. B* 52 (1995) 4728.
- [47] A.L. Efros, *Phys. Rev. B* 46 (1992) 7448.
- [48] J. Qi, C. Mao, J.M. White, A.M. Belcher, *Phys. Rev. B* 68 (2003) 125319.
- [49] S.A. Empedocles, R. Neuhauser, K. Shimizu, M.G. Bawendi, *Adv. Mater.* 11 (1999) 1243.
- [50] S.A. Empedocles, R. Neuhauser, M.G. Bawendi, *Nature* 399 (1999) 126.
- [51] F. Koberling, U. Kolb, I. Potapova, G. Philipp, T. Basche, *J. Phys. Chem. B* (2003) 7463.
- [52] I. Chung, K.T. Shimizu, M.G. Bawendi, *Proc. Indian Natn. Sci. Acad.* 100 (2003) 405.
- [53] V. Klimov, P. Haring Bolivar, H. Kurz, *Phys. Rev. B* 53 (1995) 1463.
- [54] C. Burda, S. Link, M. Mohamed, M. El-Sayed, *J. Phys. Chem. B* 105 (2001) 12286.